# Dynamic Topography Across the Canadian Arctic and Implications for Plio-Pleistocene Glacial Inception

Sophie Coulson[a,b,*], Mark J Hoggard[a,c,d], Fred Richards[a,e], Jacqueline Austermann[c], Jerry X. Mitrovica[a]

[a] *Department of Earth and Planetary Sciences, Harvard University, Cambridge, MA, USA*
[b] *Now at Fluid Dynamics and Solid Mechanics Group, Los Alamos National Laboratory, Los Alamos, NM, USA*
[c] *Lamont-Doherty Earth Observatory, Columbia University, Palisades, NY, USA*
[d] *Research School of Earth Sciences, Australian National University, Canberra, Australia*
[e] *Department of Earth Science & Engineering, Imperial College London, London, UK*

## 1. Introduction

Much of the topography on Earth's surface is a result of horizontal plate tectonics, which generates isostatically compensated crustal and lithospheric thickness variations. An additional component is supported by thermochemical convection in the rocky mantle, which is the ultimate driving force for plate tectonic motions, and is responsible for kilometer-scale vertical motions of the surface that evolve through time and have come to be termed 'dynamic topography' (Pekeris, 1935; Hager et al., 1985; Mitrovica et al., 1989; Gurnis, 1990). Efforts to isolate present-day dynamic topography generally involve the correction of observed topography for the isostatically compensated component of topography. These corrections yield a map of so-called 'residual topography', which is commonly used as a proxy for present-day dynamic topography (**???**)..

The presence of changes in dynamic topography have been inferred in the geological record regionally and globally using a multitude of methods. For example, in continental environments, the stratigraphic record of basin evolution has served as a primary constraint on dynamic topography through geological time (e.g. **?**Holt and Stern, 1994; Mitrovica et al., 1996; Gurnis

*Corresponding author: Sophie Coulson, slcoulson@lanl.gov

et al., 1998; Pysklywec and Mitrovica, 1999; DiCaprio et al., 2009; Daradich et al., 2002; Zahirovic et al., 2016). Moreover, undulations in ancient planation surfaces have been used to constrain the dynamic topography signal across Africa (**?**Guillocheau et al., 2018) and long-wavelength uplift across West Greenland and large areas of Eastern Canada (e.g. Japsen et al., 2006, 2016). Analyses of seismic reflection data on continental shelves have allowed authors to estimate dynamic topography changes on the Indian peninsula (Richards et al., 2016), the Australian coast (Czarnota et al., 2013), and around Africa (**??**). Numerous studies have inferred vertical crustal rates using changes in river profiles and drainage systems (e.g. Roberts and White, 2010; Shephard et al., 2010; Faccenna et al., 2019), and, observations of sea-level markers, such as drowned or tilted coral reef terraces, have been explained by patterns of dynamic topography and used to estimate rates of vertical motion (e.g. DiCaprio et al., 2010; Austermann et al., 2017; Stephenson et al., 2019).

Predictions of dynamic topography through time can be computed from mantle convection simulations by combining estimates of present-day mantle density structure derived from seismic tomography and/or subduction histories with mantle viscosity profiles (Braun, 2010; Flament et al., 2013). Dynamic topography is predicted either from the calculated normal stresses at a fixed surface or by tracking the motion of a free surface. Most simulations of this type use backwards advection schemes. These calculations begin with present-day mantle density structure and move backward through time by solving the governing equations for mantle convection in a forward sense but with the sign of gravity reversed, typically assimilating a reconstruction of plate velocities for surface boundary conditions (e.g Conrad and Gurnis, 2003; Moucha et al., 2008). A limitation of this methodology is that, since thermal diffusion cannot be simply reversed, it is neglected. Alternatively, this problem can be overcome using an inverse approach called the adjoint method, in which an initial condition is refined by iteratively solving the forward and backward adjoint equations and minimizing a misfit function (usually between the calculated present-day temperature structure and an observational estimate obtained from seismic tomography; Bunge et al., 2003; Liu and Gurnis, 2008; Ghelichkhan and Bunge, 2021). Adjoint methods are significantly more computationally expensive than backward advection; the two approaches are described and compared in the review of Flament et al. (2013).

As observations of dynamic topography have increased and numerical modeling of thermochemical convection has improved, a new direction of research has emerged targeting outstanding issues in ice-age paleoclimate (Mitrovica et al., 2020). Several recent studies have focused on disentangling the changes in elevation generated by dynamic topography from long term sea-level variations (e.g. Conrad, 2013; Rowley et al., 2013; Austermann et al., 2017; Stephenson et al., 2019; Richards et al., 2020a). Others have shown that accurately reconstructing bedrock topography by correcting for changes in dynamic topography is essential for assessing the stability of marine-based ice sheets during periods of relative ice-age warmth (Gomez et al., 2010; Austermann et al., 2015). Finally, the absolute elevation of ice sheets and glaciers is directly proportional to temperature (and therefore ablation rates), and snowfall patterns can be strongly influenced by variations in topography.

An important, enigmatic problem in ice-age paleoclimate involves what led to the inception of Northern Hemispheric ice at $\sim$2.7 Ma, when the Laurentide Ice Sheet began to grow from snow cover persisting year-round in high-elevation regions of the Canadian Arctic and/or Greenland. Analysis of deep-sea sedimentary core records has established the presence of major continental ice sheets in the Northern Hemisphere beginning 3.4–2.4 Ma (Shackleton et al., 1984; Jansen et al., 1990; Haug et al., 1999; Mudelsee and Raymo, 2005). Despite reasonable consensus on the timing of the onset of glaciation, the exact driver of this glacial inception has remained elusive. General circulation models, coupled ocean-atmosphere models, and ice sheets models which apply climate perturbations generated by a number of large-scale tectonic processes that are proposed to be drivers of the glacial inception (e.g. Ruddiman and Kutzbach, 1989; Raymo and Ruddiman, 1992; Keigwin, 1982; Haug and Tiedemann, 1998; Cane and Molnar, 2001; Philander and Fedorov, 2003), have either failed to simulate the patterns of snow expansion present in the geological record or have required artificial cooling to initiate glaciation (Lunt et al., 2008; Jochum et al., 2012; Birch et al., 2017).

Recent studies have begun to examine the role of long-timescale, solid-Earth processes in pushing the climate system to a more favorable state for ice growth in regions of glacial inception. Daradich et al. (2017), following DONN and SHAW (1977), argued that true polar wander (TPW), the motion of the Earth's rotation axis relative to the surface, and continental drift have moved the North American continent to increasingly higher latitudes over the last 40 Myr. This change in latitude had the effect of cooling local climate in Baffin Island and priming it for glacial inception. Solgaard et al.

(2013) argued that two phases of large-scale uplift (beginning ~10 Ma and ~5 Ma), as inferred from peneplanation surfaces and relative dating of exhumation (Bonow et al., 2006; Japsen et al., 2006), raised the topography of the Greenland mountains. This process produced an orographically-induced increase in precipitation and cooling of surface temperatures, allowing ice to accumulate during both of these periods. Using geodynamical modelling, Steinberger et al. (2015) posited that a combination of TPW, continental drift and dynamic topography preconditioned glacial inception in Greenland at ~3 Ma. Specifically, they reconstructed changes in dynamic topography since 5 Ma using a backward advection framework with a suite of density and viscosity models. Their predictions yielded uplift on the order of ~60 m $Myr^{-1}$ along the eastern coast of Greenland, and therefore regional cooling of surface temperatures since 5 Ma.

There is confounding evidence on the geographic location and synchronicity of the onset of Northern Hemispheric glaciation at ~3 Ma. Geomorphological studies (e.g. Bierman et al., 2016; Pedersen et al., 2019) and analysis of ice rafted debris records from off-shore Greenland (e.g. Larsen et al., 1994; Tripati and Darby, 2018) suggest minor glaciation may have occurred in Southern Greenland as early as ~7 Ma. However, widespread, full ice sheet growth likely did not occur until after ~2.5 Ma (Bierman et al., 2016; Pedersen et al., 2019), beginning from gradual accumulation in the southeast of Greenland (Contoux et al., 2015). Glaciation across Baffin Island may have occurred prior to this time. Hall and King (1989) observed the appearance ice-rafted debris in Baffin Bay at ~3.4 Ma, based on rock-magnetic stratigraphy of Ocean Drilling Project core 645. Cosmogenic nuclide analysis of till and regolith beneath glaciers in Northern Baffin Island suggest the area has been under continuous glacial cover for over 3 million years (Staiger et al., 2006). Moreover, Birchfield et al. (1982) used climate modeling to argue that the high elevation in parts of Baffin Island made the area susceptible to glacial inception by increasing the local sensitivity to insolation forcing. Finally, both sediment core records (Clark et al., 1993) and high-resolution, regional climate modeling (Birch et al., 2017), suggest that Baffin Island was the inception site for North American glaciation at the end of the Last Interglacial (~116 ka).

Despite an expanding number of observational constraints on dynamic topography and improved modelling techniques, dynamic topography across the Arctic remains poorly constrained (Shephard et al., 2014), especially during the Plio-Pleistocene. In this study we present a range of model-

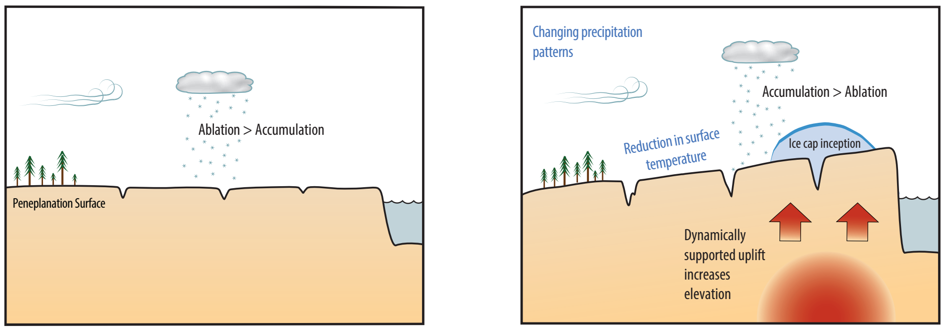


Figure 1: Schematic illustration of the potential effects of dynamic topography on surface elevation, recorded in the peneplanation surface, and implications for climate conditions.

generated dynamic topography predictions for the Canadian Arctic. We also review the geological constraints on uplift across Baffin Island. Using these constraints, we assess the magnitude and patterns of uplift generated by dynamic topography, and deduce the impact of changing topography on long-term trends in climate through the Plio-Pleistocene and the initiation of ice cover in the Northern Hemisphere. Figure 1 gives a schematic overview of the proposed affects of dynamic topography on Baffin Island, and the resulting changes in climatic conditions.

## 2. Methodology

Our backward advection-based dynamic topography predictions are generated from convection simulations using the finite-element ASPECT (Advanced Solver for Problems in Earth's ConvecTion) code. ASPECT solves the coupled equations governing conservation of mass, momentum, and energy in a compressible, momentum free mantle (Bangerth et al., 2018, 2020; Kronbichler et al., 2012; Heister et al., 2017). Mantle convective flow is driven by buoyancy (lateral density) variations, which are inferred from a mapping between perturbations in seismic velocity and density, and are resisted by the viscosity of mantle material. To predict DT changes in the past, we run our convection simulations backwards in time from present-day conditions to 5 Ma, by reversing the sign of gravity and ignoring heat diffusion across boundary layers. The time varying normal stresses at the upper boundary of the model are then mapped into changes in surface topography.

We generate predictions using five whole-mantle models. In each case, upper mantle buoyancy anomalies above 400 km are derived from a modified version of the RHGW20 temperature and density model(Richards et al., 2020b), which accounts for anelasticity at seismic frequencies and has been demonstrated to yield acceptable fits to present-day short-wavelength dynamic topography. Unlike RHGW20, which is based exclusively on the SL2013sv global surface wave tomographic model (Schaeffer and Lebedev, 2013), the buoyancy model we adopt here is augmented with regional high-resolution tomographic studies in North America (SL2013NA; Schaeffer and Lebedev, 2014), Africa (AF2019; Celli et al., 2020), and South America and the South Atlantic Ocean (SA2019; **?**; see Richards et al., 2021 for further details). We delineate the lithosphere using the 1200 °C isothermal surface, and assume that temperature decreases linearly from the lithosphere-asthenosphere boundary to the surface.

Below 400 km, temperatures are derived from thermodynamic modelling. We assume a pyrolitic mantle composition and use Perple_X alongside the thermodynamic database of Stixrude & Lithgow-Bertelloni**?** to generate a lookup table of anharmonic shear-wave velocities and densities varying temperature by $[300, 350, ..4500]$ K and pressure by $[0., 0.1, ...140]$ GPa. At each depth, temperature-dependent discontinuities in density and seismic velocity caused by phase transitions are smoothed by adopting the median temperature derivative across a $\pm 500$°C swath either side of the geotherm. Smoothed anharmonic velocities are then corrected for anelasticity using a $Q$ profile determined using the approach of Matas & BukowinskiMatas and Bukowinski (2007), as outlined in Lu et al. (2020) and Richards et al. (2021). Having smoothed and corrected the $V_S$ lookup table, velocities from five different seismic tomographic models — (LLNL-G3D-JPS**?**; S40RTS**?**; SAVANI**?**; SEMUCB-WM1**?**; TX2011**?** — are converted into temperature, with values adjusted by a constant offset to ensure mean temperatures are consistent with a representative mantle geotherm (Schuberth et al., 2009). Note that, following Richards et al. (2021), we high pass filter the seismic velocity models within the 1000–2000 km depth in order to correct for vertical smearing of long-wavelength structure and obtain an acceptable fit to the observed long-wavelength geoid-to-topography ratio (GTR). This filtering is accomplished by multiplying the spherical harmonic coefficients, $c^{lm}$, of the velocity fields with a monotonic truncation function, $f(l)$ that increases from 0 to 1 with spherical harmonic degree according to

$$f(l) = \begin{cases} -\left(\frac{l-l_{min}}{l_{max}-l_{min}}\right)^4 + 2\left(\frac{l-l_{min}}{l_{max}-l_{min}}\right)^2, & \text{if } l \leq l_{max} \\ 1, & \text{otherwise} \end{cases}$$

where $l_{min} = 1$ is the minimum spherical harmonic degree in the truncation ($f(l) = 0$) and $l_{max} = 8$ is the maximum degree ($f(l) = 1$).

Between 300 km and 400 km depth, temperatures derived from the two parameterisations are smoothly merged by taking their weighted average.

Heat flow measurements, xenolith geochemistry, seismic velocity, gravity, and topography observations suggest that compositional and thermal density contributions approximately balance each other within the continental lithosphere(Jordan, 1978; Shapiro et al., 1999). We therefore set the density within these regions equal to the average of all external material at the relevant depth, rendering them neutrally buoyant in our simulations.

Although these whole-mantle density models give a general sense of the potential magnitudes of past dynamic topography in this region, they have relatively low spatial resolution, and so may not provide an accurate prediction of local DT variations on the spatial scale of Baffin Island (i.e. a few hundreds of kilometers). Furthermore, comparison studies have shown that different global seismic tomography models are best correlated at long wavelengths, meaning short wavelength structures may not be resolved (Becker and Boschi, 2002; Root, 2020). We have constructed three additional Earth models utilizing high resolution upper mantle shear-wave tomography models in combination with the whole-mantle models described above. Specifically, we adopt the global upper mantle and transition zone shear-wave speed model of Schaeffer and Lebedev (2013) (SL2013sv) combined with the regional North America model of Schaeffer and Lebedev (2014) (SL2013NA). The latter is calculated via inversion of the same global seismic data sets as SL2013sv, meaning the two can be combined without introducing nonphysical structure. SL2013NA also contains US Array data and is characterized by higher resolution across most of the North American continent. The Schaeffer and Lebedev models have been adopted by several recent studies of dynamic topography (e.g. Steinberger, 2016; Richards et al., 2020b), and shear wave velocity anomalies in the Canadian Arctic region are consistent with patterns evident in other tomography models (e.g. Debayle et al., 2016). This upper-mantle tomography model is then combined with lower mantle structure associated with the three whole-mantle models within ASPECT, S40RTS (Ritsema et al., 2011), Savani (Auer et al., 2014) and TX2008V1-2 (Simmons et al., 2009). In these three models, density variations in the upper 250 km of the mantle are excluded, reflecting the thick continental craton present across Canada. For each of these models we adopt the viscosity profiles paired with the global density models, as listed above. All configurations described are run with model resolution of 22 km radially and 50 km tangentially at the surface. Tests doubling this resolution yielded negligible difference in results.

In all backward advection simulations a free-slip boundary condition is applied at the core-mantle boundary and the boundary condition at Earth's surface is prescribed by present-day plate velocities given by Seton et al. (2012). Depth varying thermal conductivity, thermal expansivity and heat capacity profiles are adopted from Glišović and Forte (2015) and temperature follows an adiabat. We also adopt the radially varying gravity profile of Glišović and Forte (2015).

The convection simulations output a radial stress field at the top of the domain. DT is calculated as the compensation height that balances these stresses ($\sigma_{rr}$):

$$DT = \frac{\sigma_{rr}}{\Delta\rho.g} \tag{1}$$

Where $\Delta\rho$ is the density contrast between the crust and overlying material, e.g. sediments, water or air (Austermann and Mitrovica, 2015), and $g$ is Earth's gravity. We use plate rotations from GPLATES (Seton et al., 2012; Müller et al., 2018), along with plate outlines given by Bird (2003) to translate the dynamic topography field from each time step into it's present day coordinates. To determine changes in topography, i.e. rates of uplift/subsidence, we calculate the difference between the rotated fields.

## 3. Dynamic Topography Predictions

Figure 2 shows the range of dynamic topography predictions generated by our whole-mantle tomography-based models. Three of the four predictions show uplift across the northern tip of Baffin Island, with peak magnitudes ranging from 57-88 m uplift over the last 5 Myr. These three predictions also show a significant north-south gradient in elevation changes. The S40RTS-based model, however, shows large scale subsidence on the order of 20-65 m across the region. Predictions generated by combining these whole-mantle models with the upper mantle shear-wave tomography models of Schaeffer

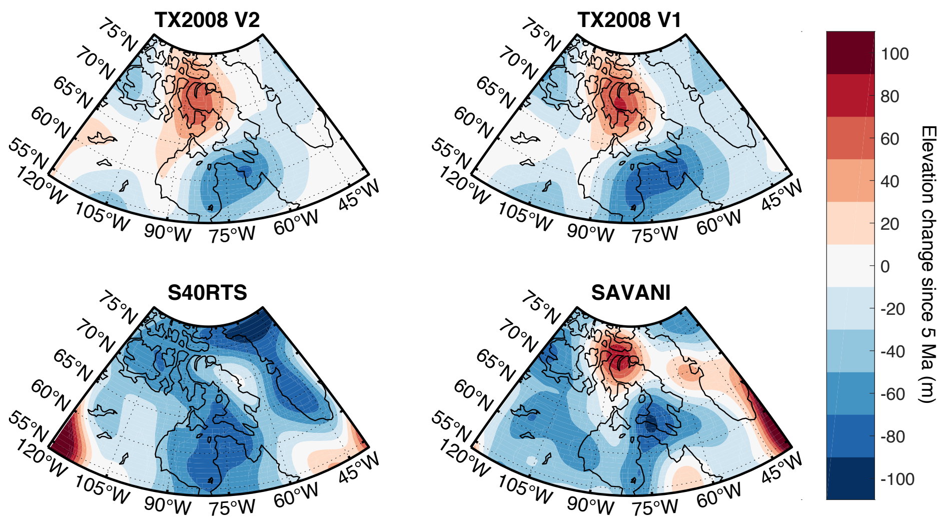


Figure 2: Predictions of dynamic topography change since 5 Ma based on the backward advection method for four whole-mantle density models inferred from shear-wave tomography, surface observables related to mantle convection and observations of glacial isostatic adjustment (top row; see text).

and Lebedev (Schaeffer and Lebedev, 2013, 2014), are shown in Figure 3. The three combined models also show uplift across northern Baffin Island and the Nunavut and Inuit Arctic Islands, with peak uplifts of 60-70 m. Again, a large gradient in elevation change is present with subsidence predicted over central and southern Baffin Island. Figure 3b demonstrates the consistency between the three combined models; they each produce similar spatial patterns of dynamic topography, with the TX2008-V1-based model producing slightly larger amplitudes in both uplift and subsidence. The majority of our whole-mantle tomography-based backward advection simulations predict subsidence across the northern portion of Quebec, as well as Labrador and across Greenland. In contrast, SAVANI and the combined models show localized areas of uplift in northern Quebec/Labrador and western Greenland.

Clearly, a variety of DT solutions are possible depending on the chosen inputs, with the choice of seismic tomography model playing a dominant role. The S40RTS tomography model is characterized by long wavelength features - i.e., a reduced magnitude of short wavelength anomalies - that arises from the significant damping applied in constructing the seismic model (Becker and

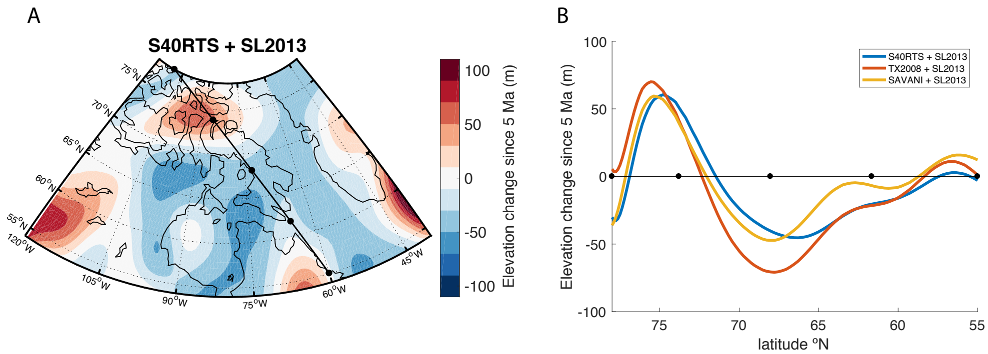


Figure 3: Predictions of dynamic topography change since 5 Ma based on the backward advection method for upper mantle density structure inferred from the shear-wave tomography of Schaeffer and Lebedev (2013, 2014). In the lower mantle, the density structure is given by one of three global mantle models shown in Figure 2. a) Spatial variation of topography change since 5 Ma for S40RTS based model (Ritsema et al., 2011), highlighting a NW-SE transect across Baffin Island. b) Elevation change across the transect shown in frame A for the three models considered (see text).

Boschi, 2002; Root, 2020). The SAVANI tomography model has adaptive resolution, from 1.25°-5°, that reflects the data sampling, with the Arctic region being a relatively low resolution area (Auer et al., 2014). Although the TX2008 model combines shear-wave speeds with a range of other geodynamic constraints, such as the global free-air gravity field, tectonic plate motions, present day DT and excess ellipticity of the core-mantle boundary (Simmons et al., 2009), it is nevertheless characterized by spatial resolution of $\sim$250 km in the shallow mantle and at the surface. The Schaeffer and Lebedev (Schaeffer and Lebedev, 2013, 2014) model offers significant improvement in resolution compared with the older whole-mantle tomography models such as S40RTS; SL2013sv has global resolution of $\sim$300 km, and the resolution of the North American component, SL2013NA, is $\sim$100-200 km. These models also require less regularization in their construction (Root, 2020).

## 4. Geological Evidence for Elevation Changes

Much of the uplift and subsidence occurring across Eastern Canada and the Canadian Arctic during the Plio-Pleistocene (5 Ma - present) can be attributed to long-wavelength mantle processes and erosion rather than active tectonics, since there is no geological evidence for tectonic activity since the cessation of sea-floor spreading in the Labrador Sea and Baffin Bay ∼35 Ma (McGregor et al., 2014). The effect of glacial isostatic adjustment is also likely small during the Pliocene as there were no major ice sheets in the Northern Hemisphere prior to Northern Hemispheric glacial inception ∼2.7 Ma.

Eastern Greenland and Baffin Island's coasts are characterized by elevated plateaus associated with uplift and exhumation. Stratigraphy shows multiple phases of uplift around Baffin Bay caused by thermal buoyancy of rifted continental margins and the isostatic response of crustal thickening during the Cenozoic (Eyles, 1996). While present-day uplifted topography in West Greenland was originally assumed to have formed at the time of rifting (36-30 Ma), recent studies have identified two subsequent episodes of uplift (11-10 Ma and 7-2 Ma) that shaped the landscape (Japsen et al., 2006; Bonow et al., 2006). This series of events is evident in changes in peneplanation surfaces (or horizontal plains that form due to rock eroding to base level during a period of uplift), and apatite fission-track dating. Initial uplift at the time of rifting led to the development of a widespread peneplanation surface across West Greenland. The second episode of uplift then elevated and tilted this surface, re-exposing it from beneath older rock cover, and initiated the formation of a second peneplanation surface. Both peneplanes were then lifted to their present-day elevations during the final stage of uplift 7-2 Ma (Japsen et al., 2006). However, these various studies do not identify a specific tectonic trigger, though they argue that uplift is not associated with any known rifting event.

Peneplanation surfaces of a similar nature, that have been tilted from their original horizontal state, are also present across Baffin Island and the Labrador coast. Bostock (1972) documents a broad, gently warped, old erosion surface that dominates the landscape in central Baffin Island. Bird (1967) and Dyke et al. (1982) describe two major peneplanation surfaces that are well represented on the Cumberland Peninsula (the southeastern tip of Baffin Island). These surfaces slope gently westward in the north of Baffin Island, and south-westward in the south (from ∼3000 ft. elevation near Barnes Ice Cap to around sea level near Foxe Plain, in the south west; Bostock, 1972). This tilt is also clearly present across the Cumberland, Hall and Frobisher Peninsulas - the southern-most three fingers of Baffin Island, east to west (Dyke et al., 1982; Bostock, 1972). A south-westward tilted peneplanation surface can be clearly identified in topographic maps and cross-sections of the area (see simplified schematic: Figure 1).

Unlike the west coast of Greenland, the ages of formation and uplift of these surfaces are largely conjectural, however, early studies suggest uplift occurred some time during the ~40 million years between the formation of the peninsulas and the Pleistocene glaciations, since rivers eroded large valleys (Dyke et al., 1982). Analysis of cosmogenic nuclide data from the Cumberland Peninsula yields erosion rates of up to 18 m/Myr over the past 2.5 Ma (Margreth et al., 2016), however this may not directly correlate with uplift. Limited apatite fission track dating of exhumation has been performed in south-east Baffin Island, though on much longer timescales than are relevant for this study (up to 440 Ma). These give exhumation rates of 7-20 m/Ma (McGregor et al., 2013; Creason, 2016).

A final potential constraint on dynamic topography comes from analyzing the spatial pattern of present-day dynamically supported highs and lows. Hoggard et al. (2017) present global maps of residual bathymetry; results for a sequence of sites in the Baffin Island region are shown in Figure 4. Red colors denote a positive anomaly in Baffin Bay. Although these results provide evidence that Baffin Bay is dynamically uplifted, they do not constrain the sign of the present-day rate of change of topography.

## 5. Implications for Long-Term Trends in Plio-Pleistocene Climate

Although the magnitude and spatial extent are not fully constrained, the DT predictions and geologic context detailed above give two independent lines of evidence for large scale uplift across north-east Baffin Island. The ongoing uplift over the last several million years has likely had a significant effect on local climate, influencing the timing and location of ice sheet growth. Glacial mass balance is governed by the rate of ice/snow accumulation and the rate of ablation, both of which are dependent on absolute elevation and patterns of topography. Ablation at a given site is directly related to surface temperatures, which are linearly proportional to elevation, and this means a simple estimate of surface temperature change can be calculated using this proportionality. Adopting a lapse rate of 5.6°C/km, taken from studies of ice sheet formation in this region (Kleman et al., 2013; Daradich et al., 2017), indicates that an 80 m increase in elevation since 5 Ma will produce a 0.45°C drop in temperature since 5 Ma. This temperature drop is comparable in magnitude to the temperature change between 1979-2010 (Foster and

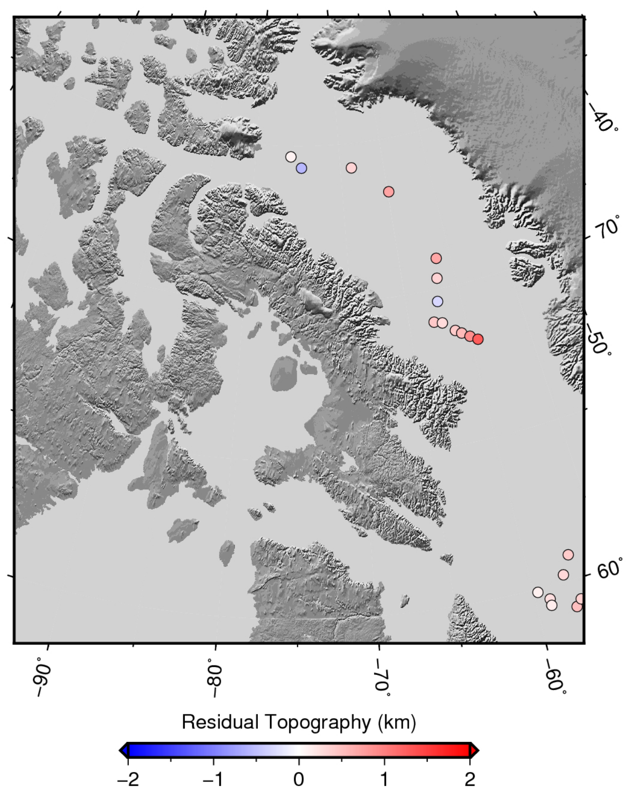


Figure 4: Residual topography across Baffin Bay with sedimentary and crustal corrections applied. Reproduced from Hoggard et al. (2017). Reds denote present day highs, blues denote lows.

Rahmstorf, 2011), during which the Greenland Ice Sheet experience mass loss of ∼2790 Gt, or ∼7.75 mm equivalent sea level (Mouginot et al., 2019).

The relationship between changes in elevation and changes in accumulation via precipitation is more complex. Some studies suggest that precipitation can be assumed to increase linearly with elevation until some maximum precipitation plateau is reached due to an "elevation desert effect" where temperature becomes too low for precipitation to form (e.g. Oerlemans, 1989). However, analysis of present-day precipitation data for the Canadian Arctic region does not show a linear relationship between elevation and precipitation. Both DT predictions and geological evidence indicate that there is a significant gradient in the long-term rate of change of topography across the island, which will also presumably play a role in altering precipitation patterns. In fact, studies of present day ice-mass changes in the Baffin Island ice caps (in particular Barnes Ice Cap, the final remnant of the Laurentide Ice Sheet in central Baffin Island) suggest that accumulation in the region may be particularly sensitive to changes in climate due to the narrow elevation range the accumulation zone covers (Gardner et al., 2012; Gilbert et al., 2017). Thus, small changes in topography may lead to non-linear changes in ice mass balance.

## 6. Summary and Outlook

Simulations of dynamic topography based on a suite of modelling methodologies and data sets predict uplift in Northern Baffin Island with peak magnitudes ranging from 57-88 m since 5 Ma. In particular, 4 out of the 5 calculations presented here show a localized region of uplift at the northern tip of Baffin Island and subsidence in the south, extending west over Hudson Bay. Tilting (northeast-southwest) across the island is supported by the presence of uplifted and tilted peneplanation surfaces documented in the geological record across central and southern Baffin Island, although a rigorous connection between our predictions and these geological features is conjectural given the lack of geochronological control on these surfaces. Across Greenland, several models presented in this study show good agreement with those of Steinberger et al. (2015), predicting uplift beneath Eastern Greenland. Although the flow mechanism driving uplift of northern Baffin Island cannot be unambiguously identified from the seismic tomography models, hot upwelling flow may be associated with remnants of a mantle plume, and/or the lateral spreading of material from the Greenland-Iceland plume beneath Baffin Bay (e.g. Gill et al., 1995; Funck et al., 2007; Peace et al., 2017).

Regardless of the mechanism, we posit that uplift in northern Baffin Island and the significant northeast-southwest gradient in elevation change across central and southern Baffin Island, predicted in most of the DT simulations described here and inferred from the geological record, likely had a substantial impact on cooling regional climate and altering snowfall patterns over the last 5 million years (Figure 1). We speculate that this process, acting in tandem with true polar wander and continental drift (Daradich et al., 2017), primed Baffin Island as the site for the inception of the Laurentide Ice Sheet. It is also possible that regional elevation changes, due to both DT and glacial isostatic adjustment (not explored here), influenced the geographic location of subsequent ice sheet growth across Northern Canada during the Pleistocene.

In this context, there are at least three areas worthy of future work. First, further mapping of peneplanation surfaces and exhumation dating of uplifted landforms on Baffin Island is required to constrain the timing and magnitude of uplift. Second, high resolution seismic and gravity studies focused on resolving features in the upper mantle beneath the Canadian Arctic would add insight into the mechanisms driving the uplift. Third, regional climate modeling that accounts for both the migration of Baffin Island northward and the time-evolving topographic gradient across the island would reveal the extent to which these geodynamic processes altered accumulation rates across the island.

## References

Auer, L., Boschi, L., Becker, T., Nissen-Meyer, T., Giardini, D., 2014. Savani: A variable resolution whole-mantle model of anisotropic shear velocity variations based on multiple data sets. Journal of Geophysical Research: Solid Earth 119, 3006–3034.

Austermann, J., Mitrovica, J., 2015. Calculating gravitationally self-consistent sea level changes driven by dynamic topography. Geophysical Supplements to the Monthly Notices of the Royal Astronomical Society 203, 1909–1922.

Austermann, J., Mitrovica, J.X., Huybers, P., Rovere, A., 2017. Detection of a dynamic topography signal in last interglacial sea-level records. Science Advances 3, e1700457.

Austermann, J., Pollard, D., Mitrovica, J.X., Moucha, R., Forte, A.M., DeConto, R.M., Rowley, D.B., Raymo, M.E., 2015. The impact of dynamic topography change on antarctic ice sheet stability during the mid-pliocene warm period. Geology 43, 927–930.

Bangerth, W., Dannberg, J., Gassmoeller, R., Heister, T., 2018. Aspect v2.0.1. URL: `https://zenodo.org/record/1297145`, doi:10.5281/ZENODO.1297145.

Bangerth, W., Dannberg, J., Gassmoeller, R., Heister, T., Others, 2020. Aspect: Advanced solver for problems in earth's convection, user manual doi:10.6084/M9.FIGSHARE.4865333.

Becker, T.W., Boschi, L., 2002. A comparison of tomographic and geodynamic mantle models. Geochemistry, Geophysics, Geosystems 3.

Bierman, P.R., Shakun, J.D., Corbett, L.B., Zimmerman, S.R., Rood, D.H., 2016. A persistent and dynamic east greenland ice sheet over the past 7.5 million years. Nature 540, 256–260.

Birch, L., Cronin, T., Tziperman, E., 2017. Glacial inception on baffin island: the role of insolation, meteorology, and topography. Journal of Climate 30, 4047–4064.

Birchfield, G., Weertman, J., Lunde, A.T., 1982. A model study of the role of high-latitude topography in the climatic response to orbital insolation anomalies. Journal of Atmospheric Sciences 39, 71–87.

Bird, J., 1967. Physiography of arctic canada, with special reference to the area south of parry channel .

Bird, P., 2003. An updated digital model of plate boundaries. Geochemistry, Geophysics, Geosystems 4.

Bonow, J.M., Japsen, P., Lidmar-Bergström, K., Chalmers, J.A., Pedersen, A.K., 2006. Cenozoic uplift of nuussuaq and disko, west greenland—elevated erosion surfaces as uplift markers of a passive margin. Geomorphology 80, 325–337.

Bostock, H., 1972. Physiographic subdivisions of canada .

Braun, J., 2010. The many surface expressions of mantle dynamics. Nature Geoscience 3, 825–833.

Bunge, H.P., Hagelberg, C., Travis, B., 2003. Mantle circulation models with variational data assimilation: inferring past mantle flow and structure from plate motion histories and seismic tomography. Geophysical Journal International 152, 280–301.

Cane, M.A., Molnar, P., 2001. Closing of the indonesian seaway as a precursor to east african aridification around 3–4 million years ago. Nature 411, 157–162.

Celli, N.L., Lebedev, S., Schaeffer, A.J., Gaina, C., 2020. African cratonic lithosphere carved by mantle plumes. Nature Communications 11, 1–10. doi:10.1038/s41467-019-13871-2.

Clark, P., Clague, J., Curry, B.B., Dreimanis, A., Hicock, S., Miller, G., Berger, G., Eyles, N., Lamothe, M., Miller, B., et al., 1993. Initiation and development of the laurentide and cordilleran ice sheets following the last interglaciation. Quaternary Science Reviews 12, 79–114.

Conrad, C.P., 2013. The solid earth's influence on sea level. Bulletin 125, 1027–1052.

Conrad, C.P., Gurnis, M., 2003. Seismic tomography, surface uplift, and the breakup of gondwanaland: Integrating mantle convection backwards in time. Geochemistry, Geophysics, Geosystems 4.

Contoux, C., Dumas, C., Ramstein, G., Jost, A., Dolan, A., 2015. Modelling greenland ice sheet inception and sustainability during the late pliocene. Earth and Planetary Science Letters 424, 295–305.

Creason, C., 2016. Phanerozoic exhumation history of hall peninsula, baffin island: Insights from apatite and zircon (u-th-sm)/he thermochronology and 3d thermokinematic modeling .

Czarnota, K., Hoggard, M., White, N., Winterbourne, J., 2013. Spatial and temporal patterns of cenozoic dynamic topography around australia. Geochemistry, Geophysics, Geosystems 14, 634–658.

Daradich, A., Huybers, P., Mitrovica, J.X., Chan, N.H., Austermann, J., 2017. The influence of true polar wander on glacial inception in north america. Earth and Planetary Science Letters 461, 96–104.

Daradich, A., Pysklywec, R., Mitrovica, J., 2002. Mantle flow modeling of the anomalous subsidence of the silurian baltic basin. Geophysical research letters 29, 20–1.

Debayle, E., Dubuffet, F., Durand, S., 2016. An automatically updated s-wave model of the upper mantle and the depth extent of azimuthal anisotropy. Geophysical Research Letters 43, 674–682.

DiCaprio, L., Gurnis, M., Müller, R.D., 2009. Long-wavelength tilting of the australian continent since the late cretaceous. Earth and Planetary Science Letters 278, 175–185.

DiCaprio, L., Müller, R.D., Gurnis, M., 2010. A dynamic process for drowning carbonate reefs on the northeastern australian margin. Geology 38, 11–14.

DONN, W.L., SHAW, D.M., 1977. Model of climate evolution based on continental drift and polar wandering. Geological Society of America Bulletin 88, 390–396.

Dyke, A.S., Andrews, J.T., Miller, G.H., 1982. Quaternary geology of cumberland peninsula, baffin island, district of franklin .

Eyles, N., 1996. Passive margin uplift around the north atlantic region and its role in northern hemisphere late cenozoic glaciation. Geology 24, 103–106.

Faccenna, C., Glišović, P., Forte, A., Becker, T.W., Garzanti, E., Sembroni, A., Gvirtzman, Z., 2019. Role of dynamic topography in sustaining the nile river over 30 million years. Nature Geoscience 12, 1012–1017.

Flament, N., Gurnis, M., Müller, R.D., 2013. A review of observations and models of dynamic topography. Lithosphere 5, 189–210.

Foster, G., Rahmstorf, S., 2011. Global temperature evolution 1979–2010. Environmental research letters 6, 044022.

Funck, T., Jackson, H.R., Louden, K.E., Klingelhöfer, F., 2007. Seismic study of the transform-rifted margin in davis strait between baffin island (canada) and greenland: What happens when a plume meets a transform. Journal of Geophysical Research: Solid Earth 112.

Gardner, A., Moholdt, G., Arendt, A., Wouters, B., 2012. Accelerated contributions of canada's baffin and bylot island glaciers to sea level rise over the past half century. The Cryosphere 6, 1103–1125.

Ghelichkhan, S., Bunge, H.P., 2021. Global mantle flow retrodictions for the early cenozoic using an adjoint method: evolving dynamic topographies, deep mantle structures, flow trajectories and sublithospheric stresses. Geophysical Journal International In Review.

Gilbert, A., Flowers, G., Miller, G., Refsnider, K., Young, N., Radić, V., 2017. The projected demise of barnes ice cap: evidence of an unusually warm 21st century arctic. Geophysical Research Letters 44, 2810–2816.

Gill, R., Holm, P., Nielsen, T., 1995. Was a short-lived baffin bay plume active prior to initiation of the present icelandic plume? clues from the high-mg picrites of west greenland. Lithos 34, 27–39.

Glišović, P., Forte, A.M., 2015. Importance of initial buoyancy field on evolution of mantle thermal structure: Implications of surface boundary conditions. Geoscience Frontiers 6, 3–22.

Gomez, N., Mitrovica, J.X., Huybers, P., Clark, P.U., 2010. Sea level as a stabilizing factor for marine-ice-sheet grounding lines. Nature Geoscience 3, 850–853.

Guillocheau, F., Simon, B., Baby, G., Bessin, P., Robin, C., Dauteuil, O., 2018. Planation surfaces as a record of mantle dynamics: the case example of africa. Gondwana Research 53, 82–98.

Gurnis, M., 1990. Bounds on global dynamic topography from phanerozoic flooding of continental platforms. Nature 344, 754–756.

Gurnis, M., Müller, R.D., Moresi, L., 1998. Cretaceous vertical motion of australia and the australianantarctic discordance. Science 279, 1499–1504.

Hager, B.H., Clayton, R.W., Richards, M.A., Comer, R.P., Dziewonski, A.M., 1985. Lower mantle heterogeneity, dynamic topography and the geoid. Nature 313, 541–545.

Hall, F., King, J., 1989. Rock-magnetic stratigraphy of site 645 (baffin bay) from odp leg 105, in: Proceedings of the Ocean Drilling Program, Scientific Results, pp. 843–859.

Haug, G.H., Sigman, D.M., Tiedemann, R., Pedersen, T.F., Sarnthein, M., 1999. Onset of permanent stratification in the subarctic pacific ocean. Nature 401, 779–782.

Haug, G.H., Tiedemann, R., 1998. Effect of the formation of the isthmus of panama on atlantic ocean thermohaline circulation. Nature 393, 673–676.

Heister, T., Dannberg, J., Gassmöller, R., Bangerth, W., 2017. High accuracy mantle convection simulation through modern numerical methods–ii: realistic models and problems. Geophysical Journal International 210, 833–851.

Hoggard, M.J., Winterbourne, J., Czarnota, K., White, N., 2017. Oceanic residual depth measurements, the plate cooling model, and global dynamic topography. Journal of Geophysical Research: Solid Earth 122, 2328–2372.

Holt, W., Stern, T., 1994. Subduction, platform subsidence, and foreland thrust loading: The late tertiary development of taranaki basin, new zealand. Tectonics 13, 1068–1092.

Jansen, E., Sjøholm, J., Bleil, U., Erichsen, J., 1990. Neogene and pleistocene glaciations in the northern hemisphere and late miocene—pliocene global ice volume fluctuations: evidence from the norwegian sea, in: Geological history of the polar oceans: Arctic versus Antarctic. Springer, pp. 677–705.

Japsen, P., Bonow, J.M., Green, P.F., Chalmers, J.A., Lidmar-Bergström, K., 2006. Elevated, passive continental margins: Long-term highs or neogene uplifts? new evidence from west greenland. Earth and Planetary Science Letters 248, 330–339.

Japsen, P., Green, P.F., Bonow, J.M., Hinchey, A.M., Wilton, D.H., 2016. Burial and exhumation history of the labrador-newfoundland margin: first observations. Geological Survey of Denmark and Greenland (GEUS) Bulletin 35, 91–94.

Jochum, M., Jahn, A., Peacock, S., Bailey, D.A., Fasullo, J.T., Kay, J., Levis, S., Otto-Bliesner, B., 2012. True to milankovitch: glacial inception in the new community climate system model. Journal of Climate 25, 2226–2239.

Jordan, T.H., 1978. Composition and development of the continental tectosphere. Nature 274, 544–548.

Keigwin, L., 1982. Isotopic paleoceanography of the caribbean and east pacific: role of panama uplift in late neogene time. Science 217, 350–353.

Kleman, J., Fastook, J., Ebert, K., Nilsson, J., Caballero, R., 2013. Pre-lgm northern hemisphere ice sheet topography. Climate of the Past 9, 2365–2378.

Kronbichler, M., Heister, T., Bangerth, W., 2012. High accuracy mantle convection simulation through modern numerical methods. Geophysical Journal International 191, 12–29.

Larsen, H., Saunders, A., Clift, P., Beget, J., Wei, W., Spezzaferri, S., 1994. Seven million years of glaciation in greenland. Science 264, 952–955.

Liu, L., Gurnis, M., 2008. Simultaneous inversion of mantle properties and initial conditions using an adjoint of mantle convection. Journal of Geophysical Research: Solid Earth 113.

Lu, C., Forte, A.M., Simmons, N.A., Grand, S.P., Kajan, M.N., Lai, H., Garnero, E.J., 2020. The Sensitivity of Joint Inversions of Seismic and Geodynamic Data to Mantle Viscosity. Geochemistry, Geophysics, Geosystems 21, e2019GC008648.

Lunt, D.J., Foster, G.L., Haywood, A.M., Stone, E.J., 2008. Late pliocene greenland glaciation controlled by a decline in atmospheric co 2 levels. Nature 454, 1102–1105.

Margreth, A., Gosse, J.C., Dyke, A.S., 2016. Quantification of subaerial and episodic subglacial erosion rates on high latitude upland plateaus: Cumberland peninsula, baffin island, arctic canada. Quaternary Science Reviews 133, 108–129.

Matas, J., Bukowinski, M.S., 2007. On the anelastic contribution to the temperature dependence of lower mantle seismic velocities. Earth and Planetary Science Letters 259, 51–65.

McGregor, E., Nielsen, S., Stephenson, R., Haggart, J.W., 2014. Basin evolution in the davis strait area (west greenland and conjugate east baffin/labrador passive margins) from thermostratigraphic and subsidence modelling of well data: Implications for tectonic evolution and petroleum systems. Bulletin of Canadian Petroleum Geology 62, 311–329.

McGregor, E., Nielsen, S., Stephenson, R., Petersen, K., MacDonald, D., 2013. Long-term exhumation of a palaeoproterozoic orogen and the role of pre-existing heterogeneous thermal crustal properties: a fission-track study of se baffin island. Journal of the Geological Society 170, 877–891.

Mitrovica, J., Austermann, J., Coulson, S., Creveling, J., Hoggard, M., Jarvis, G., Richards, F., 2020. Dynamic topography and ice age paleoclimate. Annual Review of Earth and Planetary Sciences 48.

Mitrovica, J., Beaumont, C., Jarvis, G., 1989. Tilting of continental interiors by the dynamical effects of subduction. Tectonics 8, 1079–1094.

Mitrovica, J., Pysklywec, R., Beaumont, C., Rutty, A., 1996. The devonian to permian sedimentation of the russian platform: An example of subduction-controlled long-wavelength tilting of continents. Journal of Geodynamics 22, 79–96.

Moucha, R., Forte, A.M., Mitrovica, J.X., Rowley, D.B., Quéré, S., Simmons, N.A., Grand, S.P., 2008. Dynamic topography and long-term sea-level variations: There is no such thing as a stable continental platform. Earth and Planetary Science Letters 271, 101–108.

Mouginot, J., Rignot, E., Bjørk, A.A., Van den Broeke, M., Millan, R., Morlighem, M., Noël, B., Scheuchl, B., Wood, M., 2019. Forty-six years of greenland ice sheet mass balance from 1972 to 2018. Proceedings of the National Academy of Sciences 116, 9239–9244.

Mudelsee, M., Raymo, M.E., 2005. Slow dynamics of the northern hemisphere glaciation. Paleoceanography 20.

Müller, R.D., Cannon, J., Qin, X., Watson, R.J., Gurnis, M., Williams, S., Pfaffelmoser, T., Seton, M., Russell, S.H., Zahirovic, S., 2018. Gplates: building a virtual earth through deep time. Geochemistry, Geophysics, Geosystems 19, 2243–2261.

Oerlemans, J., 1989. On the response of valley glaciers to climatic change, in: Glacier fluctuations and climatic change. Springer, pp. 353–371.

Peace, A.L., Foulger, G.R., Schiffer, C., McCaffrey, K.J., 2017. Evolution of labrador sea–baffin bay: plate or plume processes? Geoscience Canada , 91–102.

Pedersen, V.K., Larsen, N.K., Egholm, D.L., 2019. The timing of fjord formation and early glaciations in north and northeast greenland. Geology 47, 682–686.

Pekeris, C.L., 1935. Thermal convection in the interior of the earth. Geophysical Journal International 3, 343–367.

Philander, S.G., Fedorov, A.V., 2003. Role of tropics in changing the response to milankovich forcing some three million years ago. Paleoceanography 18.

Pysklywec, R.N., Mitrovica, J.X., 1999. The role of subduction-induced subsidence in the evolution of the karoo basin. The Journal of Geology 107, 155–164.

Raymo, M.E., Ruddiman, W.F., 1992. Tectonic forcing of late cenozoic climate. Nature 359, 117–122.

Richards, F., Coulson, S., Austermann, J., Hoggard, M., Mitrovica, J.X., 2020a. Impact of dynamic topography on late cenozoic sea-level records: Examples from australia, in: AGU Fall Meeting 2020, AGU.

Richards, F., Hoggard, M., Ghelichkhan, S., Koelemeijer, P., Lau, H., 2021. Geodynamic, geodetic, and seismic constraints favour deflated and dense-cored llvps .

Richards, F., Hoggard, M., White, N., 2016. Cenozoic epeirogeny of the indian peninsula. Geochemistry, Geophysics, Geosystems 17, 4920–4954.

Richards, F.D., Hoggard, M.J., White, N., Ghelichkhan, S., 2020b. Quantifying the relationship between short-wavelength dynamic topography and thermomechanical structure of the upper mantle using calibrated parameterization of anelasticity. Journal of Geophysical Research: Solid Earth 125, e2019JB019062.

Ritsema, J., Deuss, a.A., Van Heijst, H., Woodhouse, J., 2011. S40rts: a degree-40 shear-velocity model for the mantle from new rayleigh wave dispersion, teleseismic traveltime and normal-mode splitting function measurements. Geophysical Journal International 184, 1223–1236.

Roberts, G.G., White, N., 2010. Estimating uplift rate histories from river profiles using african examples. Journal of Geophysical Research: Solid Earth 115.

Root, B., 2020. Comparing global tomography-derived and gravity-based upper mantle density models. Geophysical Journal International 221, 1542–1554.

Rowley, D.B., Forte, A.M., Moucha, R., Mitrovica, J.X., Simmons, N.A., Grand, S.P., 2013. Dynamic topography change of the eastern united states since 3 million years ago. science 340, 1560–1563.

Ruddiman, W.F., Kutzbach, J.E., 1989. Forcing of late cenozoic northern hemisphere climate by plateau uplift in southern asia and the american west. Journal of Geophysical Research: Atmospheres 94, 18409–18427.

Schaeffer, A., Lebedev, S., 2013. Global shear speed structure of the upper mantle and transition zone. Geophysical Journal International 194, 417–449.

Schaeffer, A., Lebedev, S., 2014. Imaging the north american continent using waveform inversion of global and usarray data. Earth and Planetary Science Letters 402, 26–41.

Schuberth, B.S., Bunge, H.P., Ritsema, J., 2009. Tomographic filtering of high-resolution mantle circulation models: Can seismic heterogeneity be explained by temperature alone? Geochemistry, Geophysics, Geosystems 10.

Seton, M., Müller, R.D., Zahirovic, S., Gaina, C., Torsvik, T., Shephard, G., Talsma, A., Gurnis, M., Turner, M., Maus, S., et al., 2012. Global continental and ocean basin reconstructions since 200 ma. Earth-Science Reviews 113, 212–270.

Shackleton, N.J., Backman, J., Zimmerman, H., Kent, D.V., Hall, M., Roberts, D.G., Schnitker, D., Baldauf, J., Desprairies, A., Homrighausen, R., et al., 1984. Oxygen isotope calibration of the onset of ice-rafting and history of glaciation in the north atlantic region. Nature 307, 620–623.

Shapiro, S.S., Hager, B.H., Jordan, T.H., 1999. The continental tectosphere and Earth's long-wavelength gravity field. Lithos 48, 135–152.

Shephard, G., Flament, N., Williams, S., Seton, M., Gurnis, M., Müller, R., 2014. Circum-arctic mantle structure and long-wavelength topography since the jurassic. Journal of Geophysical Research: Solid Earth 119, 7889–7908.

Shephard, G., Müller, R., Liu, L., Gurnis, M., 2010. Miocene drainage reversal of the amazon river driven by plate–mantle interaction. Nature Geoscience 3, 870–875.

Simmons, N.A., Forte, A.M., Grand, S.P., 2009. Joint seismic, geodynamic and mineral physical constraints on three-dimensional mantle heterogeneity: Implications for the relative importance of thermal versus compositional heterogeneity. Geophysical Journal International 177, 1284–1304.

Solgaard, A.M., Bonow, J.M., Langen, P.L., Japsen, P., Hvidberg, C.S., 2013. Mountain building and the initiation of the greenland ice sheet. Palaeogeography, Palaeoclimatology, Palaeoecology 392, 161–176.

Staiger, J.W., Gosse, J., Little, E.C., Utting, D.J., Finkel, R., Johnson, J.V., Fastook, J., 2006. Glacial erosion and sediment dispersion from detrital cosmogenic nuclide analyses of till. Quaternary Geochronology 1, 29–42.

Steinberger, B., 2016. Topography caused by mantle density variations: observation-based estimates and models derived from tomography and lithosphere thickness. Geophysical Supplements to the Monthly Notices of the Royal Astronomical Society 205, 604–621.

Steinberger, B., Spakman, W., Japsen, P., Torsvik, T.H., 2015. The key role of global solid-earth processes in preconditioning greenland's glaciation since the pliocene. Terra Nova 27, 1–8.

Stephenson, S.N., White, N.J., Li, T., Robinson, L.F., 2019. Disentangling interglacial sea level and global dynamic topography: analysis of madagascar. Earth and Planetary Science Letters 519, 61–69.

Tripati, A., Darby, D., 2018. Evidence for ephemeral middle eocene to early oligocene greenland glacial ice and pan-arctic sea ice. Nature communications 9, 1–11.

Zahirovic, S., Flament, N., Dietmar Müller, R., Seton, M., Gurnis, M., 2016. Large fluctuations of shallow seas in low-lying s outheast a sia driven by mantle flow. Geochemistry, Geophysics, Geosystems 17, 3589–3607.